JOURNAL OF CATALYSIS 145, 194–203 (1994)

La–Eu Cuprates as Catalysts for Phenol Oxidation

Lucio Forni,[1] Cesare Oliva,* Anatoli V. Vishniakov,† Alexei M. Ezerets,† Ivan E. Mukovozov,† Francesco P. Vatti,* and Vera N. Zubkovskaja†

*Dipartimento di Chimica Fisica ed Elettrochimica, Università di Milano, Via C. Golgi 19, 20133 Milan, Italy; and †D. I. Mendeleev Moscow University of Chemical Technology, Miusskaja Square 9, Moscow, Russia

Received November 24, 1992; revised April 28, 1993

A set of six $La_{2-x}Eu_xCuO_{4+\delta}$ oxides were prepared, with x ranging from 0 to 1.33. They were characterized by various techniques, including, in addition to chemical analysis, surface area and porosity measurements, XRD, SEM-EPMA, EPR, and electric resistivity measurements. All the oxides proved to be good catalysts for the oxidation of phenol with hydrogen peroxide and, under proper reaction conditions, a high selectivity to *p*-benzoquinone was obtained with each solid. Different selectivities to hydroquinone or to catechol were also obtained, depending on the value of x. The best catalytic performance was obtained in any case at relatively low temperatures (≤70°C). Increasing the temperature beyond 70°C led only to fast wasting of hydrogen peroxide and to faster oxidation of the products to CO_2, without any advantage on yield to the desired products. A competition exists between the reactants for adsorption on the same surface sites. Phenol is adsorbed very strongly, although it can be displaced rather easily by hydrogen peroxide. The results of the characterization analysis indicate that catalytic activity is very probably connected with the presence of Cu ions forming anisotropic quantum spin fluid (AQSF) or glass (AQSG) structures. When the catalyst becomes inactive, AQSF and AQSG disappear and strongly oxygen-deficient copper clusters form. © 1994 Academic Press, Inc.

INTRODUCTION

Mixed oxides of general formula A_2BO_4, A and B being a trivalent and a bivalent transition metal ion, respectively, are known to be active oxidation catalysts. This is true especially when their formula is changed to $A_{2-x}C_xBO_4$, C being a second bivalent, trivalent, or tetravalent transition metal ion. Examples of the partial substitution of C for A are given by Nitadori and Misono in $La_{2-x}Sr_xCoO_4$ (1) and $La_{2-x}Sr_xNiO_4$ (2). Yamazoe and Teraoka (3) studied the difference in catalytic behavior for partial oxidation of two series of catalysts of A_2BO_4 structure ($La_{2-x}Sr_xCoO_4$) and of ABO_3 structure ($La_{1-x}Sr_xCoO_3$). They concluded that activity and selectivity of these perovskite-like catalysts may be correlated with oxygen deficiency. Rajadurai *et al.* (4) tried to correlate the catalytic activity of $La_{2-x}Sr_xCuO_4$ for CO oxidation with some physicochemical parameters of the catalyst, such as electrical conductivity, lattice parameters, oxygen vacancies, etc. The catalytic activity showed a volcano-shaped trend as a function of x, with a maximum for $x = 0.4$. A study of the activity of some alkaline-earth cuprates for the oxidation of alkylaromatics was carried out also by our research group (5).

When C is a trivalent or a tetravalent metal ion, the resulting structure may contain layers of a particular A_2BO_4 oxide structure, intergrown with layers of a different structure. An example is given by Manthiran and Goodenough (6). They found that in $La_{2-x}Nd_xCuO_4$ the orthorhombic structure of La_2CuO_4 not only undergoes a displacive transition to tetragonal symmetry, but also becomes unstable, relative to the Nd_2CuO_4 T′-tetragonal structure, giving rise to a new, slightly different T″-tetragonal phase.

The oxidation of phenol (PH) by H_2O_2 (HP) is a widely applied process in chemical industry for the preparation of the dihydroxylated derivatives, namely hydroquinone (HQ) and catechol (CA). This oxidation process is frequently reported as taking place through the decomposition of HP, with formation of an unstable electrophilic intermediate, which attacks the PH nucleus to give a PHO^- ion. The latter can be considered as the precursor of the products (HQ and CA) usually forming by this process. However, in the presence of an oxidizing species, HQ transforms into quinhydrone (QH), also named semiquinone radical (SQR) or, in its dissociated form, semiquinone radical anion (SQRA) (7, 8). This reaction is favoured at low pH, where QH is also unstable. The formation of QH was detected by EPR (7) at pH = 3.7 during the reaction of HQ and HP, catalyzed by peroxidase. A strongly pH-dependent EPR spectrum was detected, due to protonation of the SQRA, resulting in the formation of the SQR. Stable radical species were observed in the case of formation of radical chelate com-

[1] To whom correspondence should be addressed.

0021-9517/94 $5.00
Copyright © 1994 by Academic Press, Inc.
All rights of reproduction in any form reserved.

plexes of CA with metal cations such as Y^{3+} or La^{3+} in water (9). Hückel calculations also indicated (9) that the ionization potential from HQ to QH (SQR or SQRA) and from the latter to BQ increases with increasing the strength of the metal bonding. This results in a stabilization of the paramagnetic SQR or SQRA species.

Both homogeneous (10–13) and heterogeneous (14–20) catalysts have been proposed or are in commercial use for the oxidation of PH with HP. All the papers and patents on the subject exclude the presence of resorcinol among the reaction products, except in one case (19) in which the reaction was carried out at a temperature as high as 400°C. It has also been found that the distribution of the products is affected by the nature of the solvent: in protic solvents, such as methanol, HQ prevails over CA (20), while in aprotic solvents, such as acetone or butanone, CA prevails over HQ.

In the present work we have characterized some mixed oxides of the general formula $La_{2-x}Eu_xCuO_4$ and have used them as catalysts for the oxidation of PH with HP in heterogeneous liquid–solid phase, looking for possible correlations between activity, selectivity and physicochemical characteristics of the catalyst.

EXPERIMENTAL

Catalysts

Six different catalysts were prepared by adding under vigorous stirring a solution of citric acid (1.33 g equivalents per 1 g equivalent of metals) and ethylene glycol (5 cm^3 per 1 g of the final oxide mixture) to a hot solution of La, Eu, and Cu nitrates in the desired ratios. The resulting solution was evaporated under stirring until formation of a gel. The latter was cautiously evaporated on a hot plate up to 300°C to remove any organic matter. The resulting solid was finely ground and calcined in air up to 920°C for 7 h, ground again, and calcined at 1000°C for 4 h.

Catalyst Characterization

The composition of the catalyst has been determined by standard chemical analysis methods. The oxygen excess was evaluated by iodometric titration as suggested in Ref. (21). The presence or absence of known crystalline phases was checked by XRD on a Siemens D-500 diffractometer, employing the Debye method (Cu $K\alpha$ radiation, Ni-filtered) and comparing the patterns so obtained with literature data (22). Morphology and surface composition were analyzed by SEM-EPMA with a Cambridge Stereoscan 150 instrument coupled with a Link Mod.860 apparatus. EPMA analysis was done by integrating the counts for a preset lifetime and for a large number of different positions over the sample at various magnifications. Electrical resistivity was measured by the standard dc four-terminal method. BET surface area and porosity were determined by N_2 adsorption–desorption on a Sorptomatic 1800 C.Erba apparatus. EPR analysis was carried out by a Bruker EST-300 EPR-ENDOR instrument, equipped with a temperature-controlling device. The samples were finely ground and transferred into open-to-atmosphere sample holders. Relevant characteristics of the catalysts employed are collected in Table 1.

TABLE 1

Characteristics of the Catalysts Employed

Catalyst no.	Composition	Value of δ (± 0.005)	Surface area m^2/g	Pore volume cm^3/g
1	$La_{0.67}Eu_{1.33}CuO_{4+\delta}$	0.008	0.9	0.14
2	$LaEuCuO_{4+\delta}$	0.011	<0.1	0.04
3	$La_{1.33}Eu_{0.67}CuO_{4+\delta}$	0.013	0.1	0.04
4	$La_{1.67}Eu_{0.33}CuO_{4+\delta}$	0.016	8.9	0.28
5	$La_{1.85}Eu_{0.15}CuO_{4+\delta}$	0.016	13.0	0.98
6	$La_2CuO_{4-\delta}$	0.010	0.3	0.06

Catalytic Reactor

The activity-comparison tests were carried out in a 100 cm^3 semicontinuous stirred-tank (SCSTR) glass reactor, equipped with reflux condenser, thermostatic jacket, thermometer, metering pump for feeding the second reactant, and a port for pipetting analytical samples. A few additional tests were carried out by means of a temperature-programmed desorption–reaction (TPDR) apparatus equipped with a UTI-100 quadrupolar mass spectrometric (QMS) detector, described in detail elsewhere (23), using helium as carrier gas.

Procedure and Analysis

(*a*) *SCSTR runs.* The solution (25 cm^3) of the first reactant (PH) in acetone + water (80/12/8 = PH/acetone/water weight ratios) was placed in the reactor and brought to the desired reaction temperature under stirring. After addition of the desired amount of finely ground catalyst powder, the metering pump for the dropwise addition of the second reactant (HP, 35 wt% aqueous solution) was started (reaction time $t = t_0$). The analytical samples (0.3 g, corresponding to ca. 0.3 cm^3) were pipetted at the desired time intervals. The final (the so-called $t = \infty$) sampling was taken 30 to 60 min after the last drop of the HP solution was added.

The gas-chromatographic (GC) analysis was made on a FID HP 5710 apparatus, equipped with a silanized glass column, 2.2 m long, 6 × 2 mm in diameter, packed with 80/100 mesh Supelco Carbopack C/0.1% SP.1000 and op-

erated isothermally at 190°C. After careful separation of the catalyst, the remaining solution was titrated iodometrically to determine the amount of residual, unconverted HP. The CO_2 forming during the reaction was detected by bubbling the gas issuing from the reactor in $Ba(OH)_2$ solution.

(*b*) *TPDR tests*. After a fresh sample of catalyst (ca. 200 mg) was charged, it was purged *in situ* under a slow flow of ultrapure He (≥99.9999 vol%) through TPD ramps (20°C/min) from the initial 50°C to the final 500°C isothermal dwell, held for 20 min. When no more contaminants were detected in the gas leaving the reactor, the adsorption-desorption runs were carried out by injecting a pulse (ca. 3 mm^3) of reactant (PH) or of one of the products (HQ, CA, or *p*-benzoquinone, BQ), dissolved at ca. 50 wt% in acetone, during the isothermal dwell preceding the ramp. The characteristic mass fragments coming out from the reactor were continuously monitored by means of the QMS detector. The competition of the reactants in adsorption was tested either by preadsorbing PH, followed by one pulse of the HP solution, or by injecting pulses of an equimolar solution of the two reactants.

RESULTS

Chemical Analysis

The results of chemical analysis are given as stoichiometric coefficients or δ values in Table 1. The error of the iodometric titration for δ could give rise to some doubt on the position of the maximum for samples 4 and 5. However, the trend indicated by the Table 1 data may be considered reasonably safe, since each of them has been calculated by averaging the results of several titrations on different samples of every catalyst.

Analysis by SEM-EPMA

Some typical microphotographs are shown in Fig. 1. As a consequence of the high temperature of calcining, a very high degree of sintering is generally present in our samples. Indeed, in most cases (Figs. 1a–c,f) the solid particles appear as "glued" together by thick "necks" of solid material. Of course, this leads to values of BET surface area lower than 1 m^2/g. The only exceptions are perhaps samples 4 and 5 (Figs. 1d and e), the BET surface area of which is higher than 8 m^2/g (Table 1). The porosity was always lower than 1 cm^3/g. The analysis by EPMA on each sample did not show any significant difference among the ratios of the various metal ions (La, Eu, Cu) as a result of changing either the position or the width of the zone analyzed on the sample. The values of the stoichiometric coefficients found by this EPMA "surface" analysis practically matched the "bulk" ones obtained by chemical analysis (Table 1). This ensures that the composition of every sample is homogeneous, without segregation of any metal between surface and bulk.

Analysis by XRD

The analysis by XRD showed sharp and well resolved signals, indicating a good crystallinity of the material. The diffractograms of samples 5 and 6 (Fig. 2e,f) show the only presence of orthorhombic La_2CuO_4 (JCPDS file 30-487) (22). The pattern of sample 4 (Fig. 2d) begins to show also the lines of another phase, so far not reported in the JCPDS files, indicated by (□) in the figure. These lines become more evident in sample 3 (Fig. 2c), but completely disappear from the diffractograms of samples 1 and 2 (Fig. 2a,b). The latter show only the lines characteristic of the tetragonal Eu_2CuO_4 phase (JCPDS file 22–234). This is due to the rather different ionic radius of La^{3+} and Eu^{3+} (1.15 and 1.03 Å, respectively), preventing the accommodation of La^{3+} ions in Eu_2CuO_4 or of Eu^{3+} ions in the La_2CuO_4 framework structure (24). Indeed, the partial substitution of Eu^{3+} for La^{3+} ions leads to a progressive decrease of both unit cell volume and unit cell parameters (see Fig. 3, in which the data relative to pure Eu_2CuO_4 are also given). A similar behavior was noted by others (25) when Nd^{3+} or Pr^{3+} (ionic radius 1.08 and 1.09 Å, respectively) was substituted for La^{3+} in $La_{2-x}Ln_xCuO_4$, although sometimes, just in correspondence with the crystalline phase transition, an abrupt increase of the cell parameters was observed (6). The decrease was attributed to the formation of an additional tetragonal phase, stabilized by guest ions. Similarly, we tentatively attribute the additional lines of the XRD pattern of samples 4 and 3 (Fig. 2c,d) to an usually unstable, tetragonal La-cuprate phase (T_{La}), stabilized by the presence of the intergrown tetragonal Eu-cuprate (T_{Eu}).

Analysis by EPR

(*a*) *$La_2CuO_{4+\delta}$*. The experimental EPR pattern of sample 6 (Fig. 4c) is composed of two different spectra. One of them can be attributed to Cu^{2+} ions and is similar to those observed by others (25). In our case this spectrum has been computer-simulated at 66 K (Fig. 5) with g_x = 2.165, g_y = 2.064, g_z = 2.175, and $A_x = A_y$ = 40.57 G, A_z = 80 G. However, we must emphasize that g_z and A_z have just a minor influence on the overall spectral shape, so that their evaluation should be considered only qualitative. This is probably due to the overlapping of a second, ca. 1000 G broad line, which could be consistent with an anisotropic quantum spin fluid (AQSF) state with $S = \frac{1}{2}$ (26, 27) for temperatures higher than the critical value (T_{SG}) of spin-glass formation. The anisotropic nature of the QSF, probably caused by the same defects displaying the narrower Cu^{2+} EPR line, generates an effective $S = \frac{1}{2}$ state.

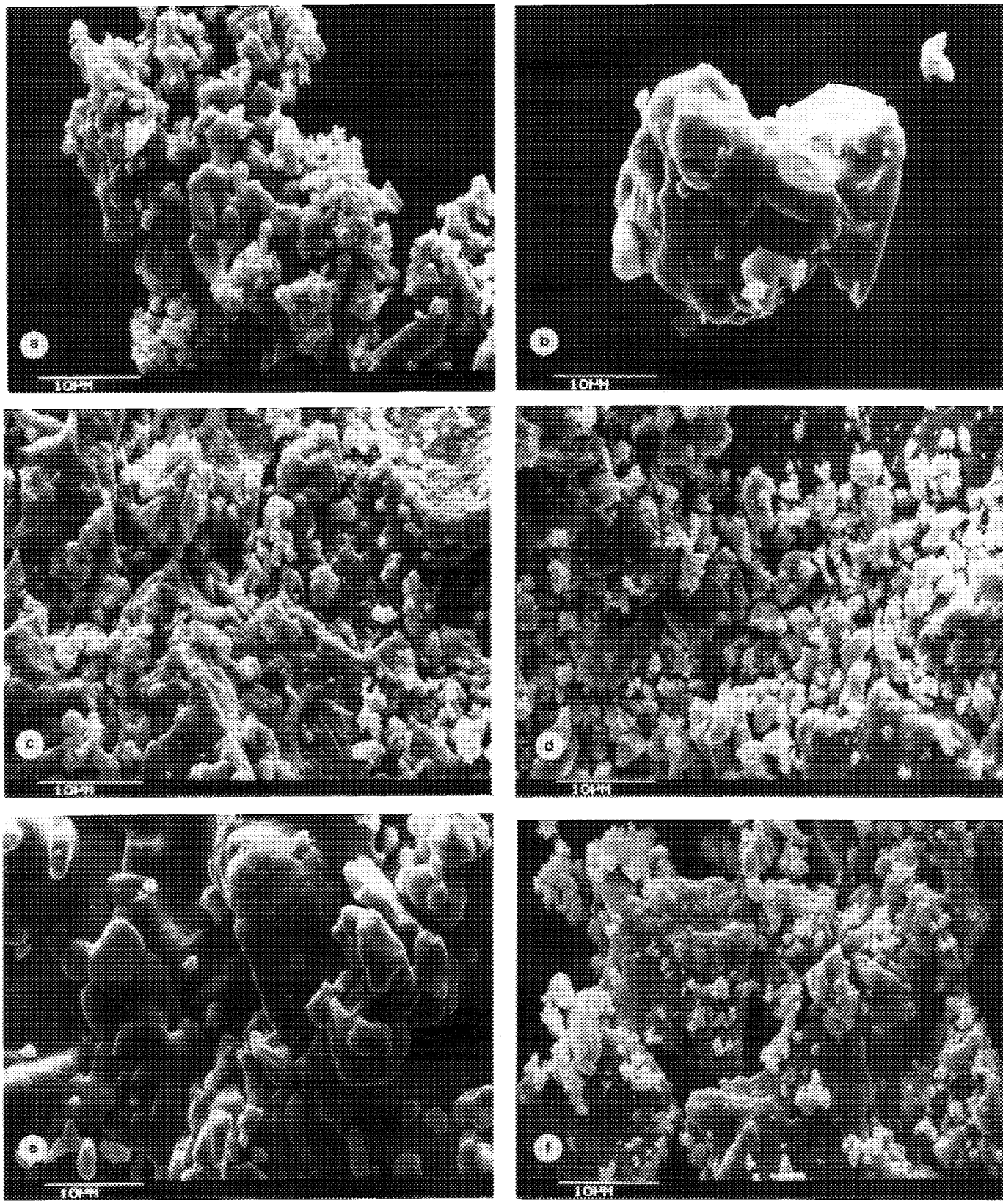

FIG. 1. Typical scanning electron micrographs of the catalysts employed. (a) to (f): catalysts Nos. 1 to 6 of Table 1.

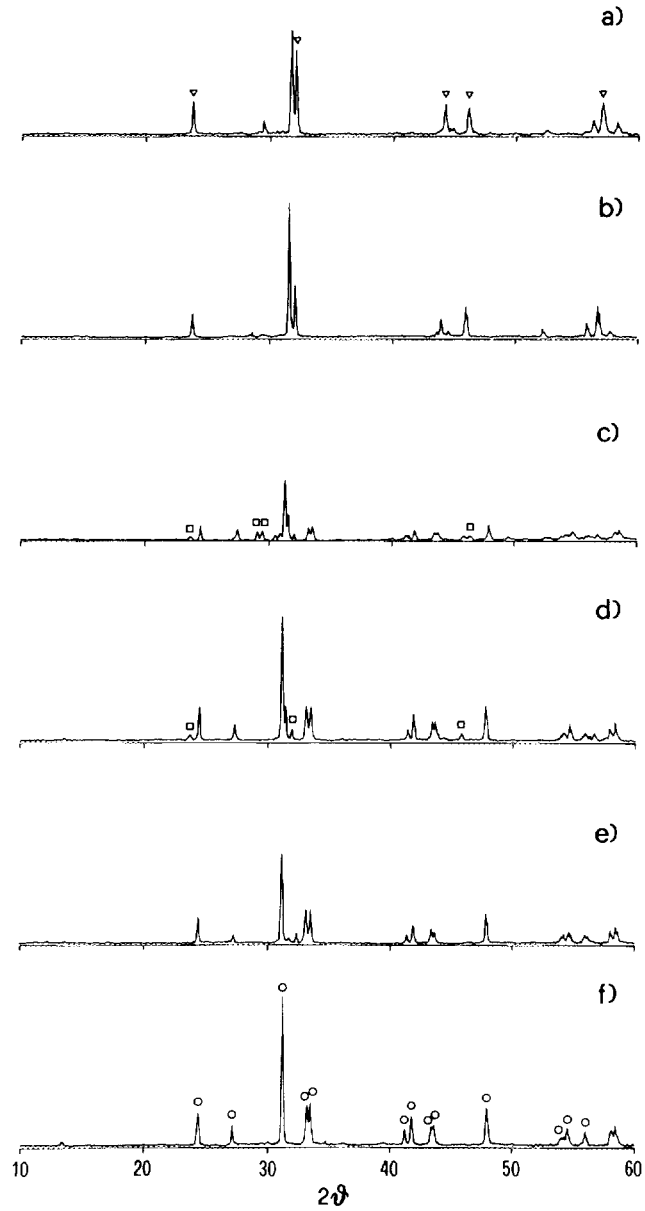

FIG. 2. XRD patterns of the catalysts employed. From (a) to (f): catalysts Nos. 1 to 6. JCPDS file Nos: (▽) Eu_2CuO_4, 22-234; (○) La_2CuO_4, 30-487; (□) pattern of T_{La} phase (see text).

(*b*) $La_{2-x}Eu_xCuO_{4+\delta}$. As previously mentioned, the Eu_2CuO_4 crystal structure cannot match the orthorhombic structure of La_2BX_4 compounds (24) and a significant crystal distortion is expected with increasing x. This has been neatly observed in the present case.

A strong dependence of the shape and features of the EPR spectrum on the La/Eu ratio was noticed (Figs. 4 and 6), confirming that the progressive substitution of Eu^{3+} for La^{3+} ions in the catalyst is accompanied by a significant change in structure. Particularly, many additional fine-structure lines extend from $g \cong 1.6$ up to $g \cong 3$. These lines cannot be eliminated by further sample grinding and they can probably be attributed (25) to the formation of AQSF states almost "frozen" in particular anisotropic quantum spin glass (AQSG) states.

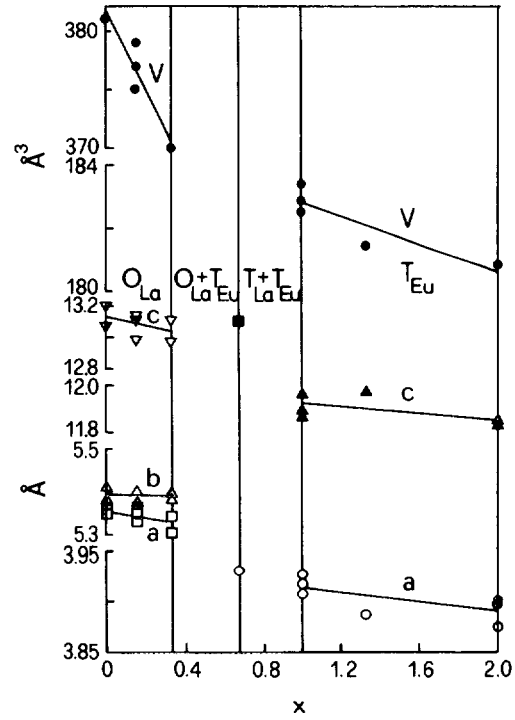

FIG. 3. Unit cell volume (V) and parameters (a, b, c) vs stoichiometric coefficient x of Eu. Data obtained at room temperature. O and T indicate orthorhombic and tetragonal structure, respectively.

(*c*) *Used catalysts.* The differences in EPR spectra due to changes in the value of x seem to smooth out after reaction. In fact, all the aged catalysts gave rather similar

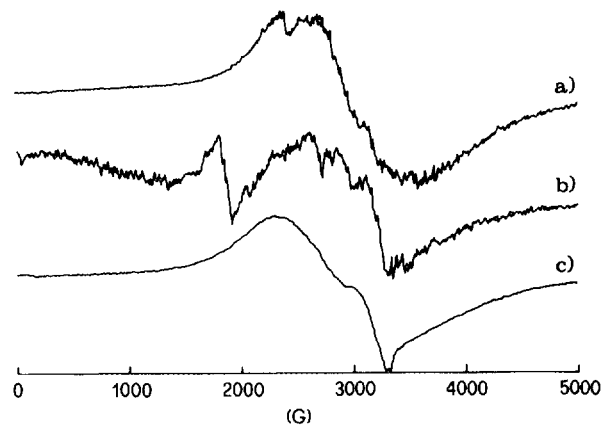

FIG. 4. From (a) to (c): EPR spectra at 300 K of catalysts Nos. 1, 4, and 6, respectively.

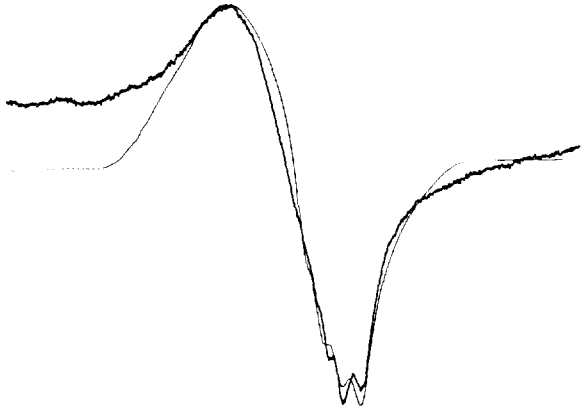

FIG. 5. Computer simulation of the EPR spectrum at 66 K of catalyst No. 6. Simulation parameters: $g_x = 2.165$, $g_y = 2.064$, $g_z = 2.175$, $A_x = A_y = 40.57$ G, $A_z = 80$ G.

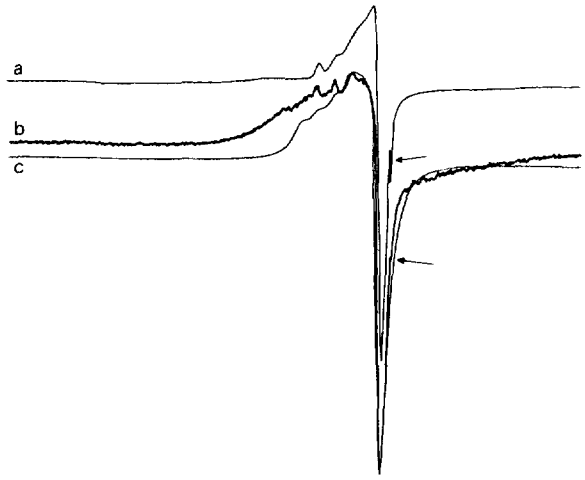

FIG. 7. (a, b) EPR spectrum of catalysts Nos. 4 and 1, respectively, after aging. (c) Computer simulation of the previous spectra. Simulation parameters: $g_x = 2.10$, $g_y = 2.075$, $g_z = 2.43$, $A_{//} = 182$ G, $A_\perp = 20.34$ G.

patterns due to isolated Cu^{2+} ions ($g_x = 2.10$, $g_y = 2.075$, $g_z = 2.43$, $A_{//} = 182$ G, $A_\perp = 20.34$ G), as shown by computer simulation (see e.g. Fig. 7c for sample 1). A second, weaker line adds to this pattern, reproducing the Lorentzian-shaped line obtained by analyzing the liquid end-product. Indeed, in both these cases a $g \cong 2$ value is measured. This feature, indicated by an arrow in Fig. 7, has also been examined in detail. Its intensity is directly proportional to the pore volume of the sample (Table 1).

(*d*) *Final liquid mixture.* A weak but stable paramagnetism was shown by the liquid mixture after reaction. A single, Lorentzian-shaped line was always observed (Fig. 8), after careful separation of the catalyst by centrifugation. At room temperature the line is characterized by $g = 2.004$ and width $= 8.4 \pm 0.5$ G. No significant change of the line was noted by changing temperature, except a slight broadening at lower temperatures.

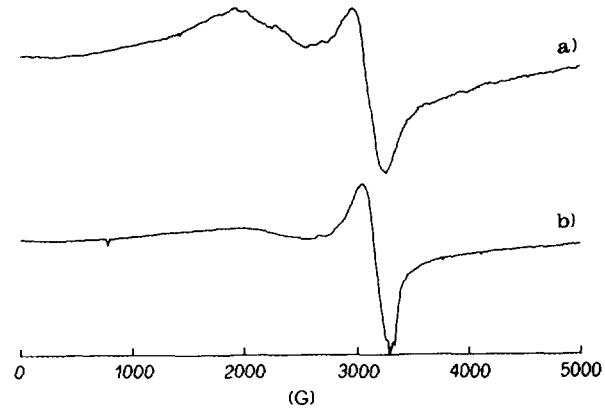

FIG. 6. EPR spectra at 66 K of catalysts Nos. 3 (a) and 6 (b).

Electrical Resistivity

The trend of electrical resistivity of our catalysts is shown in Fig. 9 as a function of the stoichiometric coefficient x of Eu. The quite low conductivity of samples 1 and 2 prevented a reasonably accurate numerical value of electrical resistivity from being measured. Hence the out-of-scale value for such samples was not included in the figure. A relatively deep minimum is noted for $x \cong 0.3$. Since all of our samples exhibit a slight but positive oxygen excess, with a maximum for $0.15 \leq x \leq 0.33$ (see Table 1), this means that a corresponding excess of positive charge must be present on metal ions and that electrical conductivity should be associated with the presence of positive holes. The latter should be connected most probably with copper ions carrying a positive charge

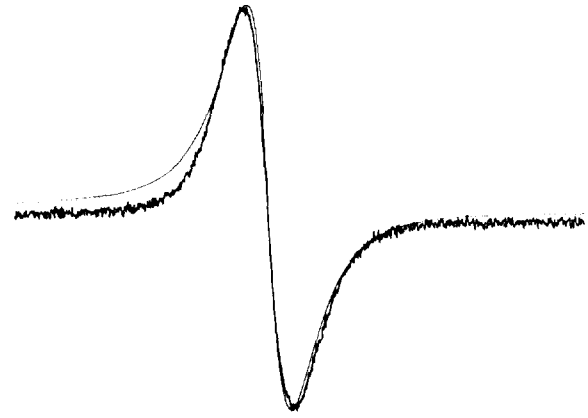

FIG. 8. Typical EPR spectrum of the liquid mixture after reaction and after separation of the catalyst. Solid line: computer-simulated Lorentzian curve.

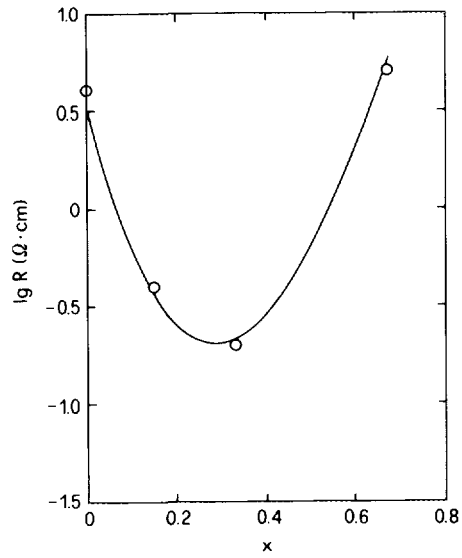

FIG. 9. Electrical resistivity of catalysts Nos. 1 to 4 vs stoichiometric coefficient x of Eu.

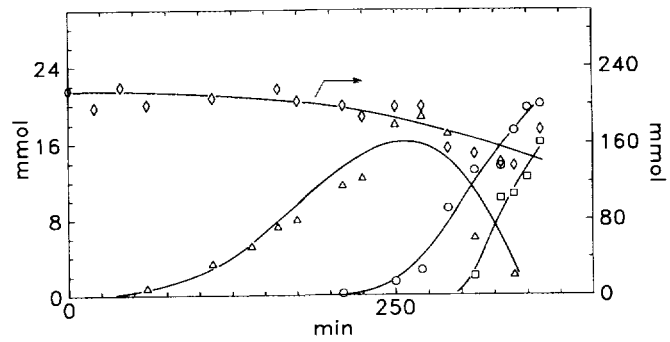

FIG. 10. Typical example of kinetic data, expressed as amount of products, (△) BQ, (○) CA, (□) HQ, and of reactant, (◇) PH, in reacting solution. Reaction temperature 70°C, catalyst No. 5.

in excess of 2, although Eu can form the rather unstable Eu^{2+} ion (ionic radius 1.12 Å). Indeed, in oxide mixtures both Cu^{+} and Cu^{3+} ions are frequently present, being easily stabilized by crystal field forces (28–30).

Catalytic Activity by SCSTR

The results of the activity test runs carried out by the SCSTR are collected in Table 2 and in Figs. 10 and 11. Practically no HP was found by iodometric titration of the final solution, which showed complete end conversion of this reactant in all runs.

Two sets of preliminary runs, not reported, were carried out in order to determine the optimal quantity of catalyst to be used and the optimal reaction temperature, respectively. In the first set three different amounts of catalyst (25, 50, 500 mg) were tried at a constant temperature of 70°C. In the first two cases the conversion was negligibly low. It was also confirmed through a blank run that no reaction occurs in the absence of catalyst, at least up to 70°C. The second set of preliminary runs, carried out at 80 and 90°C, showed that progressively faster decomposition of HP takes place with increasing temperature, with very low PH conversion and formation of tars.

All the runs of the next set (runs 1 to 6, Table 2) were carried out under identical conditions (T = 70°C, t = 6 h, stirring speed = 700 rpm, total amount of HP fed during the reaction equimolar to the charged amount of PH) in order to compare the activity of our catalysts. A typical example of the kinetic data so obtained is shown in Fig. 10. In all cases BQ was the first reaction product. Its amount grew to a maximum and then fell abruptly. Practi-

TABLE 2

Experimental Conditions and Results of Semicontinuous Stirred-Tank Reactor

Run no.	Catalyst no.	Catalyst weight, g	T, °C	HP solution feeding rate, g/min	Duration of run (min)	PH conversion %	Final content (mmol)		
							BQ	CA	HQ
1	1	0.5	70	0.058	360	58.2	—	17.9	1.52
2	2	0.5	70	0.058	360	52.8	—	18.6	2.93
3	3	0.5	70	0.058	360	48.3	—	16.9	6.87
4	4	0.5	70	0.058	360	50.0	—	18.6	4.17
5	5	0.5	70	0.058	360	36.6	—	20.3	16.10
6	6	0.5	70	0.058	360	42.3	—	18.1	5.30
7	4	0.5	70	0.055	720	66.7	—	23.9	7.10
8	5	0.5	60	0.044	540	17.4	16.8	0.34	—
9	4	0.5	60	0.044	480	27.0	28.4	1.05	—
10	4	2.0	60	0.044	480	52.7	—	17.10	10.10
11	5	2.0	70	0.044	480	52.8	—	24.20	14.30

Note. Concentration of the HP aqueous solution = 35 wt%. Stirring speed = 700 rpm. Total volume of HP solution added in each run = 19.1 cm^3 (38.2 in run 7).

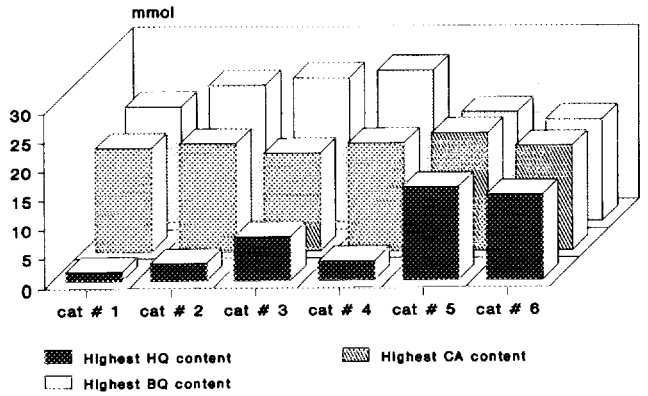

FIG. 11. Peak amount of products for runs Nos. 1 to 6 (of Table 2).

cally no BQ was found in the final reaction mixture in all these runs and the formation of CO_2 started simultaneously with the fall in amount of BQ. CA was the second-appearing reaction product and its amount always grew until the end of each run. HQ was usually detected toward the end of the reaction, though the dark color of the reaction mixture showed the presence of QH, i.e., the simultaneous presence of BQ and HQ, from the very beginning of the run. It may be inferred that HQ was quickly oxidized to the equimolar complex (BQ + HQ = 2 QH) and the latter was oxidized more easily than HQ itself, resulting in 2 mol of BQ. This can be taken as an explanation for BQ's being the first reaction product detected by GC. To be sure that QH in solution does not behave as an individual species, a solution of pure QH was prepared and analyzed by GC. No difference with respect to equimolar mixtures of HQ and BQ was noticed.

The final amount of CA was practically the same for all the catalysts. Hence, the behavior of the latter can be compared according to the highest amount of BQ or HQ measured in the reacting mixture (Fig. 11). Hence, catalyst 5 appears to be the most selective to HQ and CA and catalyst 4 the most selective to BQ. As a consequence, the next set of runs (from 7 to 11, Table 2) was performed using only these catalysts.

Run 7 was carried out with catalyst 4, in order to ascertain whether a larger amount of products could be obtained by feeding more than equimolar amounts of HP to the reacting mixture. It was found that over 8 h of reaction the amount of products did not change significantly, while the oxidation of PH proceeded, resulting only in the formation of larger amounts of CO_2.

The distribution of the reaction products was different at 60°C (runs 8 and 9). The final amounts of BQ were 28.4 and 16.8 mmol for catalysts 4 and 5, respectively. A very small amount of CA and no HQ were found in both cases; PH conversion was nearly half that at 70°C and no formation of CO_2 was noted.

The next two runs (10 and 11) show that no significant difference in PH conversion is observed, even when the amount of catalyst is increased to 2 g. Higher amounts of catalyst simply enhance the formation of CO_2 at the expense of the desired products, depressing the selectivity. Indeed, only a small difference can be noted between the results of runs 11 and 5, carried out under the same conditions, but with a fourfold different amount of the same catalyst 5. However, at 60°C the distribution of the reaction products depends significantly on the amount of catalyst (compare, e.g., runs 9 and 10).

TPDR Runs

All the catalysts behaved quite similarly in these experiments. The presaturation of the catalyst by only one reactant or product under isothermal conditions (50°C), followed by TPD, showed that PH adsorbs strongly on the catalyst surface, being desorbed only at a temperature as high as ca. 450°C (see, e.g., Fig. 12). The desorption of HQ and CA took place at much lower temperature (223°C and 150°C, respectively) and no adsorption of BQ could ever be noted.

The competition of the reactants in adsorption was examined either by presaturating the catalyst with PH, followed by one pulse of HP, or by simultaneously injecting both the reactants. It was observed that HP tends to displace PH from the catalyst surface, although not adsorbing significantly. Indeed, some PH was always detected, although in very small amounts, in the gas leaving the reactor, just after HP was injected and before the TPD ramp was started (see, e.g., Fig. 13).

DISCUSSION

In the present case only a single EPR line was observed by analyzing the liquid mixture after oxidation of PH and

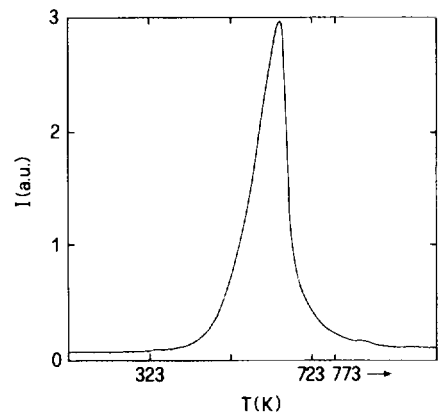

FIG. 12. Typical spectrum of temperature-programmed desorption (TPD) of PH. Ramp: 20 K/min, from 323 to 773 K.

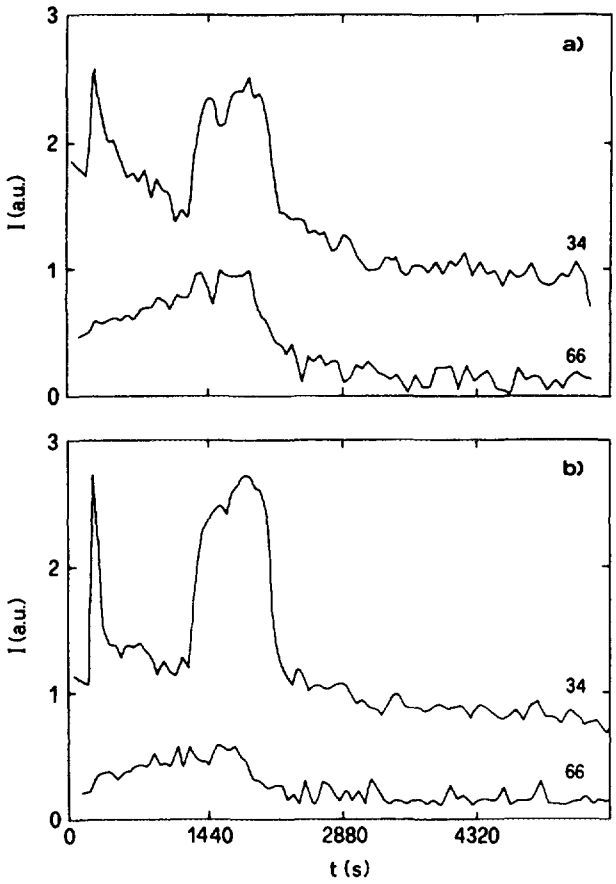

FIG. 13. Typical example of desorption of preadsorbed PH (a.m.u. = 66) after injection of HP (a.m.u. = 34). T = 323 K. (a) and (b): catalysts Nos. 5 and 4 of Table 1, respectively.

separation of the catalyst (Fig. 8). Since the pH of our reacting mixture was always of the order of 1.5, this singlet should preferably be attributed (7, 8) to the presence of SQRA species, or to association of the latter ion to metal cations, rather than to SQR species.

The rather similar EPR spectra obtained with all the catalysts after aging can be interpreted as due to isolated Cu^{2+} ions, as confirmed by computer simulation (Fig. 7c). From the optimized values of g_x, g_y, g_z, $A_{//}$, and $A_\perp$, a copper isotropic hyperfine coupling constant of 74.2 G can be calculated. The same value of the spectroscopic g-factor, characterizing both the weak line (indicated by the arrow in Fig. 7) and the line recorded with the final liquid mixture (Fig. 8), as well as the similar shape and width of such lines, suggest that they are due to the same species. Furthermore, the intensity of this weak line is directly proportional to the pore volume of the catalyst. Hence, we are led to attribute this line to the presence of organic radicals entrapped within the pore framework of the solid particles. Since repeated washing of the latter with several portions of acetone was unsuccessful in extracting such a material, a relatively high molecular weight should be attributed to these polymolecular aggregates of paramagnetic products. Alternatively, the insolubility could be due to the formation of immobilized radical chelate complexes with our metal cations.

The progressive substitution of smaller Eu^{3+} ions for La^{3+} in $La_2CuO_{4+\delta}$ brings about many physicochemical changes in the present catalysts, as described. One of the most important is the decrease of unit cell parameters and unit cell volume with increasing x (Fig. 3) accompanying the change from the original orthorhombic La-cuprate to a tetragonal La-cuprate intergrown with the tetragonal Eu-cuprate. This change in structure is accompanied also by an up to tenfold change in surface area and porosity (Table 1); by a small, but significant change in the oxygen excess (δ-parameter, Table 1); and by a noticeable change in the electrical conductivity of the solid (Fig. 9). However, not all the latter parameters vary monotonously with x. They go through a maximum with increasing x, the maxima being localized at $0.15 \leq x \leq 0.33$, i.e., for catalysts 5 and 4. This means that the distortion of the original orthorhombic structure of La-cuprate to form the intermediate tetragonal La-cuprate entrains changes not only of physical properties, such as cell parameters, surface area, and porosity, but also of chemical properties of the solid, such as the oxidation state of the metal cations.

This change is usually found when the substitution of the trivalent A-ion in the original A_2BO_4 structure is made with some differently charged metal ion, as in $La_{2-x}Sr_xCuO_4$ or in $Nd_{2-x}Ce_xCuO_4$. In those cases the change in oxidation state of the original B-ion in $A_{2-x}C_xBO_4$ is due to the change in electronic properties or in the oxide ion vacancies of the solid, brought about by the different charge on the guest C-ion. The resulting material recovers electrical equilibrium by accommodating some extra oxygen ions or by showing some oxygen deficiency.

In the present case both the La and the Eu ions are trivalent. So the only driving forces one can invoke to justify the positive values of δ are either the ability of Eu to assume the oxidation state of +2, or the crystalline field forces generated by the insertion of Eu^{3+} guest ions in the La-cuprate host structure. Our EPR data do not allow us to exclude the first hypothesis positively. However, to our knowledge, spectra due to Eu^{2+} have been observed only in a very few particular cases (31, 32). Hence, the presence of Cu^{2+} ions, revealed by the EPR spectra, coupled with the instability of the Eu^{2+} ion, lead us to accept the second hypothesis as most probable.

From a practical point of view, the most interesting result of the present work is the effect of the change of x on oxygen excess, accompanied by a change in electrical conductivity of the solid. This permits tuning of the selectivity of the present reaction toward the various products. Indeed, Fig. 11 shows that, although the "undoped" $La_2CuO_{4+\delta}$ is an active and selective catalyst, the addition

of just a small amount of Eu is sufficient to enhance the selectivity to HQ and BQ, while larger amounts are needed to increase the selectivity to CA. Another interesting result is that the activity of all the present catalysts seems to be connected with the presence of Cu ions interacting with each other through the particular environment provided by the crystalline structure of these oxide mixtures and forming AQSF or AQSG systems. When these interactions no longer exist, as shown by aged catalysts (Fig. 7), the catalytic activity ceases. This is in line with the hypothesis concerning the formation of an electrophilic intermediate after adsorption of HP. Such an intermediate can be regarded as forming on the Cu-ions, due to the ability of the latter to transfer electrons rapidly from the catalyst to the reacting species and vice versa. The previously mentioned particular environment would act as a sink of electrons, helping the active Cu-based site in the catalytic process.

REFERENCES

1. Nitadori, T., and Misono, M., *Chem. Lett.*, 1255, (1986).
2. Nitadori, T., Muramatsu, M., and Misono, M., *Bull. Chem. Soc. Jpn.* **61,** 3831 (1988).
3. Yamazoe, N., and Teraoka, Y., *Catal. Today* **8,** 175 (1990).
4. Rajadurai, S., Carberry, J. J., Li, B., and Alcock, C. B., *J. Catal.* **131,** 582 (1991).
5. Forni, L., Oliva, C., Vatti, F. P., Sinitsina, N. A., Sorochkin, S. V., Moev, A. V., and Vishniakov, A. V., *J. Chem. Soc. Faraday Trans.* **88,** 1041 (1992).
6. Manthiran, A., and Goodenough, J. B., *J. Solid State Chem.* **87,** 402 (1990).
7. Yamazaki, I., and Piette, L. H., *J. Am. Chem. Soc.* **87,** 986 (1965).
8. Smith, I. C. P., and Carrington, A., *Mol. Phys.* **12,** 439 (1967).
9. Chen, D. H., Warhurst, E., and Wilde, A. M., *J. Chem. Soc. Faraday Trans.* **63,** 2561 (1967).
10. Chawla, H. M., Sharma, S. K., Chakrabarty, K., and Bhanumati, S., *J. Chem. Soc. Chem. Commun.*, 128 (1988).
11. Lebedev, N. N., Litvintsev, I. Yu., Mitnik, Yu. V., Sapunov, V. N., Zhestov, V. A., and Aretisov, A. P., USSR Patent 1,386,309, Jan. 1988.
12. Belgian Patent BE 906,063, to Degussa, June 1987.
13. Schmall, M. W., Gorman, L. S., and Dordick, J. S., *Biochim. Biophys. Acta* **999,** 267 (1989).
14. Constantini, M., and Popa, J. M., European Patent Application, EP 299,893, Jan. 1989.
15. Bellussi, G., Clerici, M., Buonomo, F., Romano, U., Esposito, A., and Notari, B., European Patent Application EP 200,260, Dec. 1986.
16. Reddy, J. S., Kumar, R., and Rathnasamy, P., *Appl. Catal.* **58,** L1 (1990).
17. Thangaraj, A., Kumar, R., and Rathnasamy, P., *J. Catal.* **131,** 294 (1991).
18. Esposito, A., Taramasso, M., Neri, C., and Buonomo, F., UK Patent 2,116,974 (1985); Esposito, A., Neri, C., and Buonomo, F., Germany Patent DE 3,309,669, Sept. 1983; Romano, U., Esposito, A., Maspero, F., Neri, C., and Clerici, M. G., *in* "New Developments in Selective Oxidation" (G. Centi and F. Trifirò, Eds.), p. 33. Elsevier, Amsterdam, 1990.
19. Gubelmann, M., and Tirel, J., European Patent Application EP 341,164, Nov. 1989.
20. Constantini, M., Gubelmann, M., Lecomte, J. P., and Popa, J. M., European Patent Application EP 346,250, Dec. 1989.
21. Harris, D. C., and Hewston, T. A., *J. Solid State Chem.* **69,** 182 (1987).
22. Selected Powder Diffraction Data, Vols. 1–40. JCPDS, Swarthmore, PA, 1974–1992.
23. Forni, L., Toscano, M., and Pollesel, P., *J. Catal.* **130,** 392 (1991).
24. Saez Puche, R., Norton, M., and Glausinger, W. S., *Mater. Res. Bull.* **17,** 1429 (1982).
25. Singh, K. K., Ganguli, P., and Goodenough, J. B., *J. Solid State Chem.* **52,** 254 (1984).
26. Thomann, H., Klemm, R. A., Johnston, D. C., Tindall, P. J., Jin, H., and Goshorn, D. P., *Phys. Rev. B* **38,** 6552 (1988).
27. Nakamura, F., Yoshida, K., Sugiyama, K., Maeno, Y., and Fujita, T., *Physica C* **185–189,** 1103 (1991).
28. Goodenough, J. B., *Mater. Res. Bull.* **8,** 423 (1973).
29. Tranquada, J. M., Heald, S. M., Moodenbaugh, A. R., and Suenaga, M., *Phys. Rev. B* **35,** 7187 (1987).
30. Reinen, D., and Wegwerth, J., *Physica C* **183,** 261 (1991).
31. Park, S. H., Mho, S. I., and Kim, C. H., *Solid State Commun.* **83,** 47 (1992).
32. Guškos, N., Calamiotou, M., Londos, C. A., Likodimos, V., Koufoudakis, A., Mitros, C., Gamari-Seale, H., and Niarchos, D., *J. Phys. Chem. Solids* **53,** 211 (1992).